



ORIGINAL ARTICLE

Facile and sustainable synthesis of sodium lignosulfonate derived carbon quantum dots for the detection of total Mn and ascorbic acid



Tingyu Zhang^{a,b,*}, Xiaojuan Gong^b, Yi Zhang^a

^a Department of Chemistry and Chemical Engineering, Lyuliang University, Lyuliang 033000, PR China

^b Institute of Environmental Science, Shanxi University, Taiyuan 030006, PR China

Received 30 August 2022; accepted 10 November 2022

Available online 18 November 2022

KEYWORDS

SLS-CQDs;
An “on–off–on” fluorescent nanoprobe;
Mn;
Ascorbic acid

Abstract A fluorescent nanoprobe based on sodium lignosulfonate derived carbon quantum dots (SLS-CQDs) was fabricated through a facile and sustainable one-step hydrothermal treatment. The obtained SLS-CQDs had excellent fluorescence properties and were applied to detect total Mn and ascorbic acid (AA). The fluorescence of SLS-CQDs could be effectively quenched by Mn based on a static quenching process and recovered by the addition of AA. An “on–off–on” fluorescent nanoprobe was established to determine total Mn and AA with the detection limits of 6.9 µg/L and 0.65 µM with the corresponding linear ranges of 0.25–2.25, 5–25 mg/L, and 5–110 µM, respectively. This nanoprobe could accurately detect total Mn in surface water and AA in Vitamin C effervescent tablet samples. The proposed method is simple and can be performed easily, indicating that SLS-CQDs might be used in environmental monitoring, food and drug testing.

© 2022 The Author(s). Published by Elsevier B.V. on behalf of King Saud University. This is an open access article under the CC BY-NC-ND license (<http://creativecommons.org/licenses/by-nc-nd/4.0/>).

1. Introduction

Lignin is the second most abundant renewable natural biomass on earth and accounts for approximately 30 % of the organic carbon in the biosphere (Upton and Kasko, 2016). It has a wide application potential and is inexpensive, accessible, and fragrant (Kai et al., 2016; Zhu et al., 2016). As a byproduct generated in the paper/pulp

industry and the biomass refinery process (Aro and Fatehi, 2017), 50–70 million tons of lignin is produced and mainly disposed of by burning to produce thermal and electric energy (Upton and Kasko, 2016), which leads to serious secondary pollution and a huge waste of biomass. As an alternative raw material, lignin might also be used to prepare novel materials for wastewater treatment (Zhang et al., 2018; Zhang et al., 2020), high-performance catalysts for producing clean energy, and sensors for detecting chemicals (Carrier et al., 2013; Chen et al., 2013; Kibet et al., 2012), but merely accounting for 2 % (Kai et al., 2016). Therefore, developing a novel application of lignin is necessary.

Carbon quantum dots (CQDs) are advanced fluorescent carbon nanomaterials with many desirable properties (Georgakilas et al., 2015; Gong et al., 2015a; Hu et al., 2016; Jiang et al., 2015; Liu et al., 2017b). They are widely used in fluorescent sensing, biological imaging, and drug delivery (Ding et al., 2013; Gong et al., 2016;

* Corresponding author at: Department of Chemistry and Chemical Engineering, Lyuliang University, Lyuliang 033000, PR China.

E-mail address: zty@llu.edu.cn (T. Zhang).

Peer review under responsibility of King Saud University.



Kong et al., 2014; Wang et al., 2018; Zhu et al., 2022). Several studies have used lignin to prepare carbon quantum dots (Chen et al., 2016; Li et al., 2018; Liao et al., 2020; Myint et al., 2018; Niu et al., 2017; Pei et al., 2021; Yang et al., 2020; Zhu et al., 2021). Aromatic polymers are excellent precursors for preparing CQDs. They can generate high densities of electron cloud as fluorophore groups conjugating with unsaturated bonds, eventually triggering fluorescence emission. However, the types of lignin precursors mainly used in previous studies include alkali lignin (Li et al., 2018; Liao et al., 2020; Zhu et al., 2021), kraft lignin (Myint et al., 2018; Pei et al., 2021), pre-hydrolyzed lignin (Yang et al., 2020), cellulolytic enzyme lignin (Niu et al., 2017), or not mentioned (Chen et al., 2016). Additionally, the use of a doping element can effectively improve the performance of carbon quantum dots for detecting chemicals (Song et al., 2019). For example, N incorporated in the carbon matrix offers surface reaction activity, restrains non-radiative decay processes, and facilitates electron transfer (Xu et al., 2017). Instead of adding chemicals containing S, P, O, and N, lignin might be used as it contains these elements. In this study, lignosulfonate lignin containing S was used to prepare CQDs with doped S, which has rarely been investigated in previous studies. Doped S is common in CQDs, which is because the electronegativity of the S atom is similar to that of the C atom. The fabrication of CQDs is a complex process, which is due to sophisticated precursors (e.g., sodium lignosulfonate melamine formaldehyde (Pan et al., 2021) or purification processes (e.g., centrifugation, dialysis, and silica column chromatography (Rai et al., 2017; Wang et al., 2020). Thus, a simple process is required to prepare CQDs.

Manganese and ascorbic acid (AA) were selected as representative chemicals in the environment. Excessive Mn in surface water and groundwater threatens human health owing to its toxicity, bioaccumulation, persistence, and potential hazard (Abdolmohammad-Zadeh and Sadeghi, 2012; Goldhaber, 2003; Lemos et al., 2009). Various methods are used to detect Mn, including atomic absorption spectrometry (AAS) (Vieira et al., 2011), inductively coupled plasma atomic emission spectrometry (ICP-AES) (Liu et al., 2017a), inductively coupled plasma mass spectrometry (ICP-MS) (Wu et al., 2021; Zhu et al., 2019), electrochemistry (EC) (Qiu et al., 2011), etc. However, these methods are time-consuming and require expensive and bulky equipment (Najeeb et al., 2018). A simple method using fluorescence nanoparticles was developed to detect Mn species, but they responded differently to Mn(VII) (Ding et al., 2017a; Du et al., 2018a; Gong et al., 2017b; Hu et al., 2020; Liu et al., 2020a) and Mn(II) (Kumar et al., 2019; Najeeb et al., 2018; Narayanan and Han, 2017; Nie et al., 2017; Xu et al., 2021b), which led to difficulties in detecting total Mn. The amount of total Mn is an indicator of water quality for the World Health Organization (WHO) and environmental agenda in China, Japan, etc. Thus, a nanoprobe needs to be established that can be directly used for the rapid and sensitive detection of the total Mn. AA is essential for humans and is used for treating diseases, such as common cold, mental illness, infertility, and coronary heart disease (Li et al., 2014; Sun et al., 2008). Thus, detecting AA is important, which can be conducted by various CQD nanosensors (Gong et al., 2017; Song et al., 2019; Wang et al., 2021). However, better methods are needed to detect AA in samples.

In this study, we prepared sodium lignosulfonate-derived carbon quantum dots (SLS-CQDs) using a facile and sustainable one-step hydrothermal method with simple filter purification and assessed its application in the detection of total Mn and AA. The results showed that the as-synthesized SLS-CQDs exhibited high performance in detecting total Mn and AA via an “on-off-on” nanoprobe. The presence of Mn decreased the fluorescence of SLS-CQDs through a static quenching process. The addition of AA partially induced the subsequent restoration of fluorescence. We quantified the total Mn in water samples and AA in Vitamin C effervescent tablets using the SLS-CQDs.

2. Experimental

The materials and characterization are listed in the [Supplementary Material](#).

2.1. Preparation of the SLS-CQDs

Sodium lignosulfonate (0.05 g) was dissolved in ultrapure water (10 mL) under ultrasonic dispersion for 20 min, and then, EDA (0.2 mL) was added. The mixture was diverted to a 50 mL Teflon autoclave and heated up to 160 °C for 4 h. A dark brown product was obtained and purified using filter paper to remove large particles after cooling to ambient temperatures. It was further filtered through a 0.22 µm microporous membrane. Finally, the solution was lyophilized to obtain the solid products of SLS-CQDs.

2.2. Detection of total Mn based on the SLS-CQDs

The as-prepared solid products of SLS-CQDs were dissolved in ultrapure water to make a 10 mg/mL solution of SLS-CQDs. To determine the selectivity of the SLS-CQDs to Mn, some metal ions, anions, and amino acids were added to the aqueous solution of SLS-CQDs (1 mg/mL) for measuring the fluorescence intensity. To evaluate the interference of various metal ions, anions, and amino acids to Mn, the above test solution was added to 1 mg/mL of SLS-CQDs. Then, Mn was added to the above mixture, and their fluorescence intensities were recorded. Fluorescence titration was performed to obtain the linear range and detection limit of total Mn. All tests were performed at λ_{ex} of 402 nm.

2.3. Detection of AA in SLS-CQDs-Mn system

We mixed 30 mg/L of Mn with 1 mg/mL of SLS-CQDs solution to obtain the SLS-CQDs-Mn probe. By similarly introducing additional interferences, the selectivity and anti-interference efficacy toward AA was assessed (vide supra). When the excitation wavelength was at 402 nm, a fluorescence titration experiment was performed to calculate the linear range and detection limit of AA.

2.4. Pre-treatment of actual samples

All water samples were collected from Dongchuan and Beichuan rivers, Lyuliang, Shanxi, China, and immediately acidified with concentrated nitric acid to minimize precipitation and absorption on container walls. In the lab, 100 mL of water sample was digested with 5 mL of HNO₃ and 3 mL of HCl on a hot plate until the mixture was almost dried. The residue was dissolved with dilute nitric acid to 50 mL, and the pH was maintained above 1.5. Finally, the solution was filtered through a 0.45 µm microporous membrane for use.

All samples of Vitamin C effervescent tablets were purchased from a local pharmacy in Lyuliang, Shanxi, China. A tablet was weighed and dissolved in 100 mL of ultrapure water with constant stirring for about 30 min. The solution was diluted to a suitable concentration for testing.

3. Results and discussion

3.1. Characterization of the SLS-CQDs

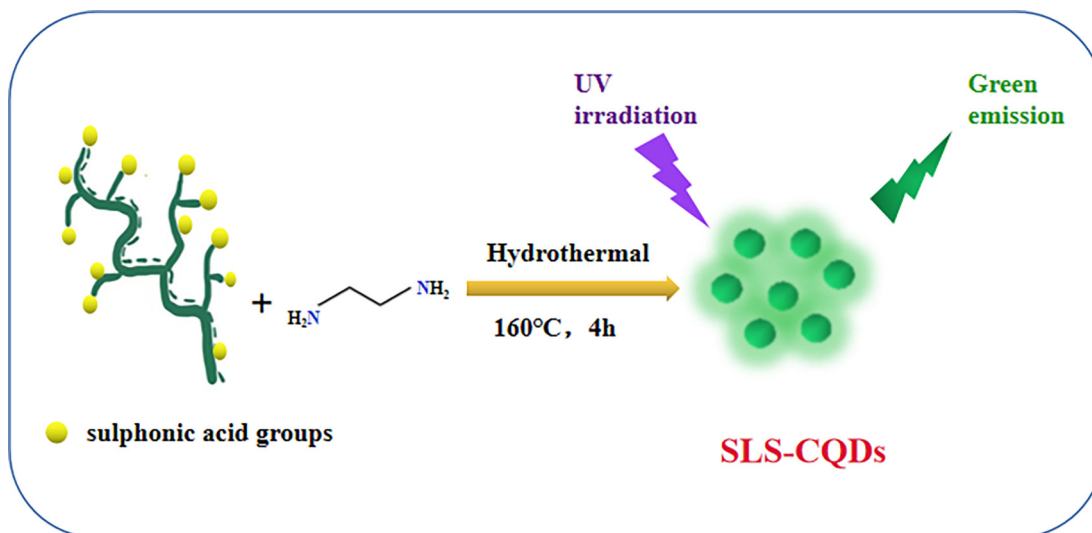
The SLS-CQDs were prepared at 160 °C for 4 h via a one-step hydrothermal route (Scheme 1). First, SLS was used as the C and S source and depolymerized under ultrasonic dispersion, followed by hydrothermal synthesis with the addition of EDA, which was the source of N. A TEM analysis (Fig. 1A) showed that the SLS-CQDs were uniformly dispersed on the copper grid, and the lattice spacing was approximately 0.34 nm. The particle size of SLS-CQDs was 1.90–6.22 nm with a mean size of 3.89 ± 0.2 nm (Fig. 1B). The SLS-CQD particles did not have an ideal spherical morphology, and the edges of the particles were irregular. This might be because SLS was folded into microspheres in the synthetic process, and carbon dot particles existed on the surface of the microspheres (Myrvold, 2008). The AFM image (Fig. 1C and 1D) showed that the average height of SLS-CQDs was 2.85 nm, and the SLS-CQDs were distributed uniformly in water. The zeta potential was -21.7 mV (Fig. S1), indicating that the SLS-CQDs were negatively charged and the system was relatively stable.

To determine the structure and surface functional groups of the SLS-CQDs, XPS, FTIR, elemental analysis, and EDX were used. As depicted in Table S1, the SLS-CQDs were composed of C 25.28, N 16.06, H 5.16, S 5.12, Na 3.69 and O (calculated) 44.69 wt%, which was similar to the composition found using EDX (Fig. S2). The empirical formula of the SLS-CQDs probably was $C_{26}H_{64}O_{35}N_{14}S_2Na_2$. The XPS survey scan (Fig. 2A) showed six binding energy peaks at 1,071.5, 531.5, 494.0, 399.5, 284.8, and 168.5 eV corresponding to Na 1s, O 1s, Na KLL, N 1s, C 1s, and S 2p, respectively. The C 1s XPS spectrum (Fig. 2B) showed five peaks at 284.5, 285.0, 285.5, 286.5, and 288.2 eV, which were related to C=C, C-C, C-N, C=N/C-O, and C=O-N, respectively (Dong et al., 2013; Liu et al., 2012). In the O 1s spectrum (Fig. 2C) the peaks at 531.7 and 532.1 eV contributed to O=C-O and C-O-C/C-OH (Chao et al., 2020). In the N 1s spectrum (Fig. 2D), the three peaks at 399.5, 400.5,

and 401.5 eV indicated amino N, pyrrolic N, and graphitic N, respectively (Chao et al., 2020; Gao et al., 2021). As depicted in Fig. 2E, S 2p had three prominent peaks at 168.0, 168.9, and 169.8 eV, which indicated C-S, S=O, and $-C-SO_x$ ($x = 2, 3,$ and 4), respectively (Gong et al., 2017b). In the FTIR spectrum (Fig. 2F), the stretching vibrations of O-H or N-H bonds ($3,447\text{ cm}^{-1}$) were detected (Yang et al., 2019). The major stretching vibration peaks of SLS were still retained in the SLS-CQDs, suggesting the presence of similar surface functional groups. The major stretching peaks for the O-H/N-H groups ($3,447\text{ cm}^{-1}$), C=O ($1,605/1,579\text{ cm}^{-1}$), C-O/C-N ($1,135\text{ cm}^{-1}$), and C-S (622 cm^{-1}) were more prominent in SLS-CQDs than in SLS (Pei et al., 2021; Xu et al., 2021c; Yang et al., 2019). The peaks of the stretching vibration of C=C=O/C=N ($2,117\text{ cm}^{-1}$), C=C ($1,485\text{ cm}^{-1}$), C-N ($1,327\text{ cm}^{-1}$), and para substitution of benzene (820 cm^{-1}) appeared on the spectra of SLS-CQDs (Gao et al., 2021; Song et al., 2019). The shift at $1,605\text{ cm}^{-1}$ could be ascribed to the evaluation of C=O, which increased the delocalization of π electrons. The increase in the intensity of O-H and N-H enabled the formation of the H bond, which decreased the bond force constant K and peak shift. These results indicated that SLS-CQDs are functionalized with nitrogen and sulfur atoms, SLS-CQDs are rich in hydrophilic groups on the surfaces, and more multiple-carbon rings are formed (Pei et al., 2021). The high content of C-N improved the fluorescence quantum yield (Zhu et al., 2021), probably due to the created lattice defects and replacement of C in the sp^2 carbon domain (Liu et al., 2020b; Zhang et al., 2016). The fluorescence quantum yield of the SLS-CQDs was 10.23 % (Fig. S3). These results suggested that SLS-CQDs are hydrophilic and stable.

3.2. Optical properties of the SLS-CQDs

As shown in Fig. 3A, a strong absorption peak at 243 nm was detected in the UV – vis absorption spectrum of SLS-CQDs (purple line), which was caused by the π - π^* transition of aromatic sp^2 domains from the carbon core (Liu et al., 2015). Additionally, a weak absorption peak at 330 nm was also



Scheme 1 A diagrammatic illustration of the fabrication of SLS-CQDs.

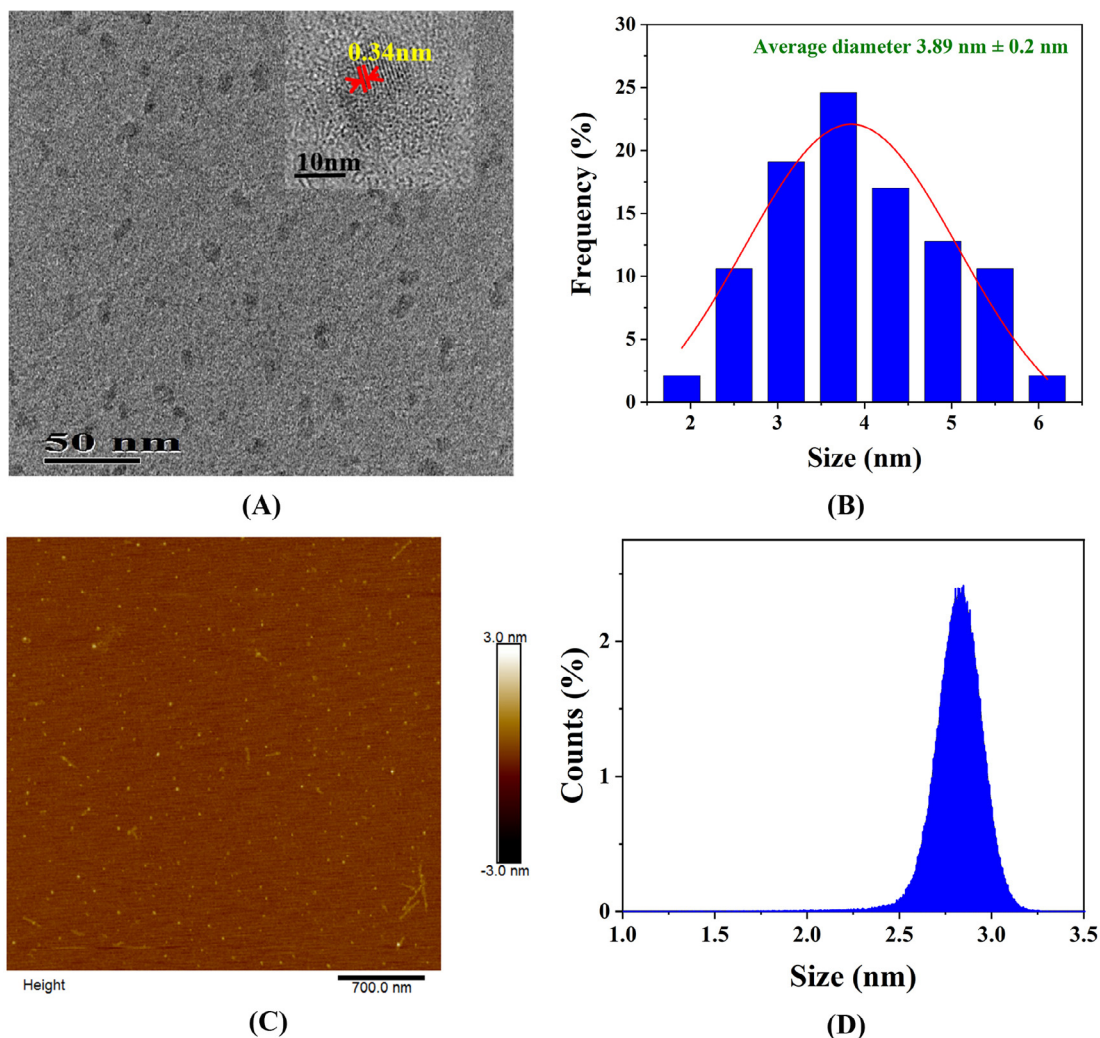


Fig. 1 (A) A TEM image, (B) a particle size distribution histogram, (C) an AFM image, and (D) the average height of the as-synthesized SLS-CQDs.

detected, induced by the $n\text{-}\pi^*$ transition of the surface moieties with nitrogen atoms (Gong et al., 2015b). The optimal excitation wavelength (green line) and emission wavelength (red line) were located at 402 nm and 492 nm, with a Stokes shift of 90 nm. From the inset photograph of Fig. 3A, the SLS-CQDs solution was found to emit bright blue-green fluorescence under 365 nm ultraviolet irradiation. Additionally, the 3D fluorescence diagram of SLS-CQDs under different λ_{ex} was studied (Fig. 3B). When the excitation wavelength moved from 350 nm to 460 nm, the emission peak was red-shifted from 476 to 519 nm. The excitation-dependent emission property is universally reported for carbon quantum dots, which is attributed to the $\pi^* \rightarrow n$ transition of the surface-attached functionalities (Dong et al., 2013; Gong et al., 2019; Gong et al., 2016).

3.3. Stability of the SLS-CQDs

The fluorescence intensity of the SLS-CQDs under conditions of changes in pH, NaCl saline solution, hydrogen peroxide (H_2O_2), UV irradiation, and xenon lamp irradiation is shown

in Fig. S4. With the increase in the NaCl concentration, the fluorescence intensity of the SLS-CQDs did not change (Fig. S4A). The effect of pH is shown in Fig. S4B; the fluorescence intensity of SLS-CQDs showed negligible changes under a wide pH range of 1.5–9.0, especially when the pH was between 1.5 and 6, and the change in the fluorescence intensity was less than 1%. The fluorescence intensity of SLS-CQDs was above 80% under 1.0 mol/L of H_2O_2 (Fig. S4C), suggesting that the as-prepared products had good antioxidant stability. After continuous UV (180 min; Fig. S4D) and xenon lamp (120 min; Fig. S4E) irradiation, the fluorescence intensity of the SLS-CQDs showed no noticeable changes, indicating favorable photostability of the SLS-CQDs.

3.4. SLS-CQDs nanoprobe for total Mn determination

To evaluate the selectivity of the system, 0.5 mM of 17 kinds of metal ions (Fig. S4A), 17 kinds of anions (Fig. S4B), and 20 kinds of amino acids (Fig. S4C) were used to produce small changes in the fluorescence intensity, except Mn^{2+} and Mn (VII). The fluorescence intensity could be quenched by both

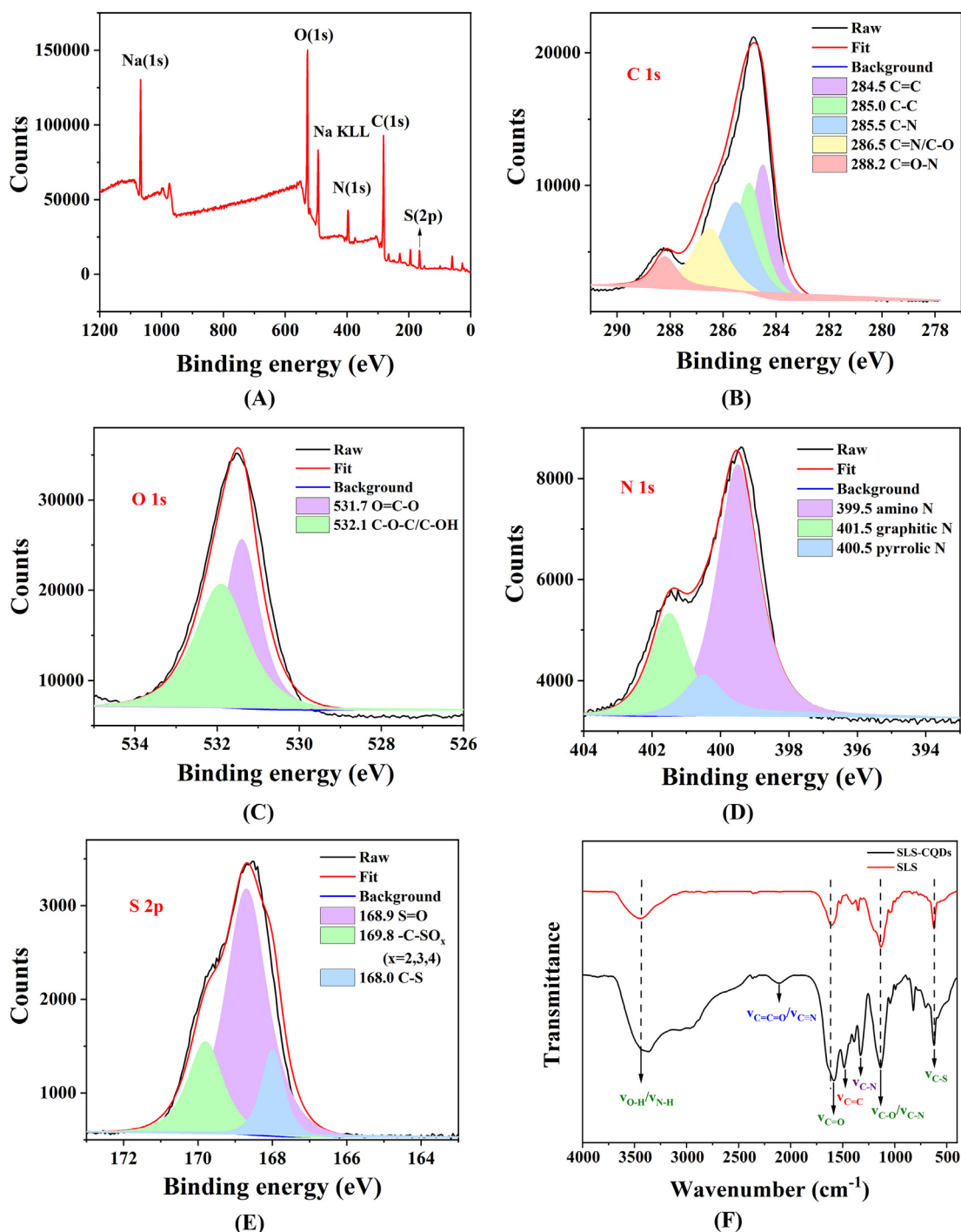


Fig. 2 (A) An XPS survey scan, (B) C 1s XPS, (C) O 1s XPS, (D) N 1s XPS, (E) S 2p XPS, and (F) FTIR spectra of SLS and SLS-CQDs.

Mn^{2+} and Mn(VII) . Subsequently, a standard solution of single Mn (1,000 mg/L) was used to determine the quenching results, which was due to the following reasons. First, the Mn standard solution was manufactured by dissolving manganese metal using nitric acid, and the solution was dominated by Mn(II). Common divalent manganese salts, such as manganese chloride, are easily oxidized in the air while being dissolved in water, which can affect the accuracy of fluorescence titration results. If acid is added to the dissolution, the pH needs to be controlled precisely, and the operation

is difficult. However, the medium of the manganese standard solution was 1.0 mol/L of HNO_3 , which could not be oxidized in the air, and the system was stable and easy to operate. Second, from the perspective of detecting total manganese in samples from the environment, the sample was acidic after digestion. The digestion process was also similar to the preparation process of the manganese standard solution which could improve the accuracy of detection. Third, manganese can exist in the form of Iron- Manganese Oxide in different environmental samples and is mainly converted to Mn(II) after diges-

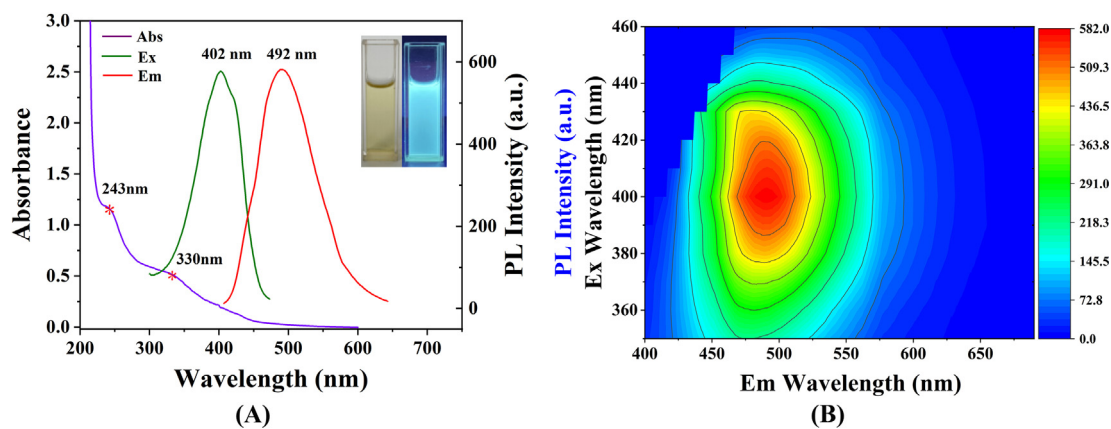


Fig. 3 (A) UV-vis absorption (purple line), fluorescence excitation (green line), and emission (red line) spectra of the SLS-CQDs (1.0 mg/mL). The inset displays images of the SLS-CQDs under daylight (left) and 365 nm UV light (right). (B) The 3D fluorescence diagram of SLS-CQDs at excitation wavelengths from 350 nm to 460 nm.

tion. Although Mn(VII) can also quench the fluorescence of SLS-CQDs, it does not interfere with the detection of total Mn in actual samples.

As the concentration of Mn increased, the fluorescence intensity decreased (Fig. 4A). Then, a nanoprobe was constructed to detect Mn based on the SLS-CQDs. The anti-interference performance of a nanoprobe is a desirable property. The high concentration (1.0 mM) of metal ions, anions, and amino acids had negligible effects on the fluorescence intensity of SLS-CQDs, whereas, the fluorescence intensity was quenched by Mn (11 mg/L, 0.2 mM, Fig. S6), which indicated that the SLS-CQDs had good anti-interference to the determination of Mn. The fluorescence titrations were used to assess the sensitivity and linear response range of the SLS-CQDs to Mn determination. The optimal concentration of SLS-CQDs was 1.0 mg/mL (Fig. S7A). The fluorescence spectra of SLS-CQDs with various concentrations of Mn are shown in Fig. 4A. With the addition of Mn from 0 to 160 mg/L, the fluorescence intensity of SLS-CQDs decreased. The equilibration time was 5 min (Fig. S7B). The titration trend diagram of SLS-CQDs with various concentrations of Mn is shown in Fig. S8. The pH decreased during titration because the medium of the standard solution of Mn was 1.0 mol/L of HNO₃. The calculated pH change was 0.80–3.60 with the concentration of Mn between 0.25 mg/L and 160 mg/L. The fluorescence intensity was almost stable when the pH was above 1.5 in the acidic environment (Fig. S4B). When the concentration of Mn reached 30 mg/L in the titration process, the pH of the solution dropped to 1.5. Therefore, to remove the interference of pH changes, 0–30 mg/L of Mn was selected to obtain the linear relationship. Two excellent linear relationships were obtained in the range of 0.25–2.5 mg/L (Fig. 4B) and 5.0–25.0 mg/L (Fig. 4C), indicating that the probing property of SLS-CQDs in the determination of total Mn was effective. The limit of detection (LOD) was calculated to be 6.9 µg/L, based on three times the standard deviation rule (1).

$$\text{LOD} = 3\sigma/S \quad (1)$$

Here, σ represents the standard deviation of six blank measurements, and S represents the slope of the calibration curve. Compared to previously reported methods for the detection of Mn (Table 1), although the LOD in this study was not lower

than the LOD in the traditional method for direct detection of Mn, the proposed SLS-CQD nanoprobe was comparable to those used in the other methods for the detection of Mn (II) or Mn(VII). However, our nanoprobe was simpler and can determine total Mn quickly and directly.

To investigate the quenching mechanism of Mn determination, the fluorescence lifetime was first evaluated. As shown in Fig. 4D and Table S2, the average fluorescence lifetime of the SLS-CQDs was 4.09 ns. When 5 mg/L of Mn was added to SLS-CQDs, the average lifetimes of SLS-CQDs was 4.10 ns. The fluorescence lifetime of SLS-CQDs remained almost unchanged with the addition of Mn, indicating that a static quenching process or the inner filter effect (IFE) might have occurred (Zu et al., 2017). The IFE occurs when the absorption spectrum of the quencher in the detection system overlaps with the excitation or emission spectra of CQDs (Zu et al., 2017). No significant overlap was observed (Fig. S9A), demonstrating that the IFE did not occur. As shown in Fig. S9B, after adding different concentrations of Mn, the disappearance of the peak of SLS-CQDs was observed at 243 nm, indicating the occurrence of static quenching. Therefore, the quenching between the interaction of SLS-CQDs and Mn was probably due to static quenching. In this quenching process, a non-fluorescent complex was formed through the interaction between SLS-CQDs and Mn (Scheme 2). Additionally, the forming complexation between Mn and reactive moieties containing N and S suppressed $\pi^* \rightarrow n$ transition, and consequently, quenched the fluorescence (Mohagheghpour et al., 2022; Xu et al., 2021a). As a hard acid, Mn(II) tended to bind to N and O atoms on SLS-CQDs, according to the HASB principles (Joshi et al., 2016; Ruan et al., 2016).

3.5. SLS-CQDs-Mn nanoprobe for AA determination

For the SLS-CQDs-Mn system, AA can partially restore the fluorescence of SLS-CQDs-Mn. The fluorescence quenching of SLS-CQDs-Mn probably occurred due to the formation of a non-fluorescent complex between SLS-CQDs and Mn, which suppressed $\pi^* \rightarrow n$ transition of the surface-attached functionalities. AA, as a complex reagent, was competitive to complex with Mn, compared with SLS-CQDs, thus decomposing the non-fluorescent complex between SLS-CQDs and Mn

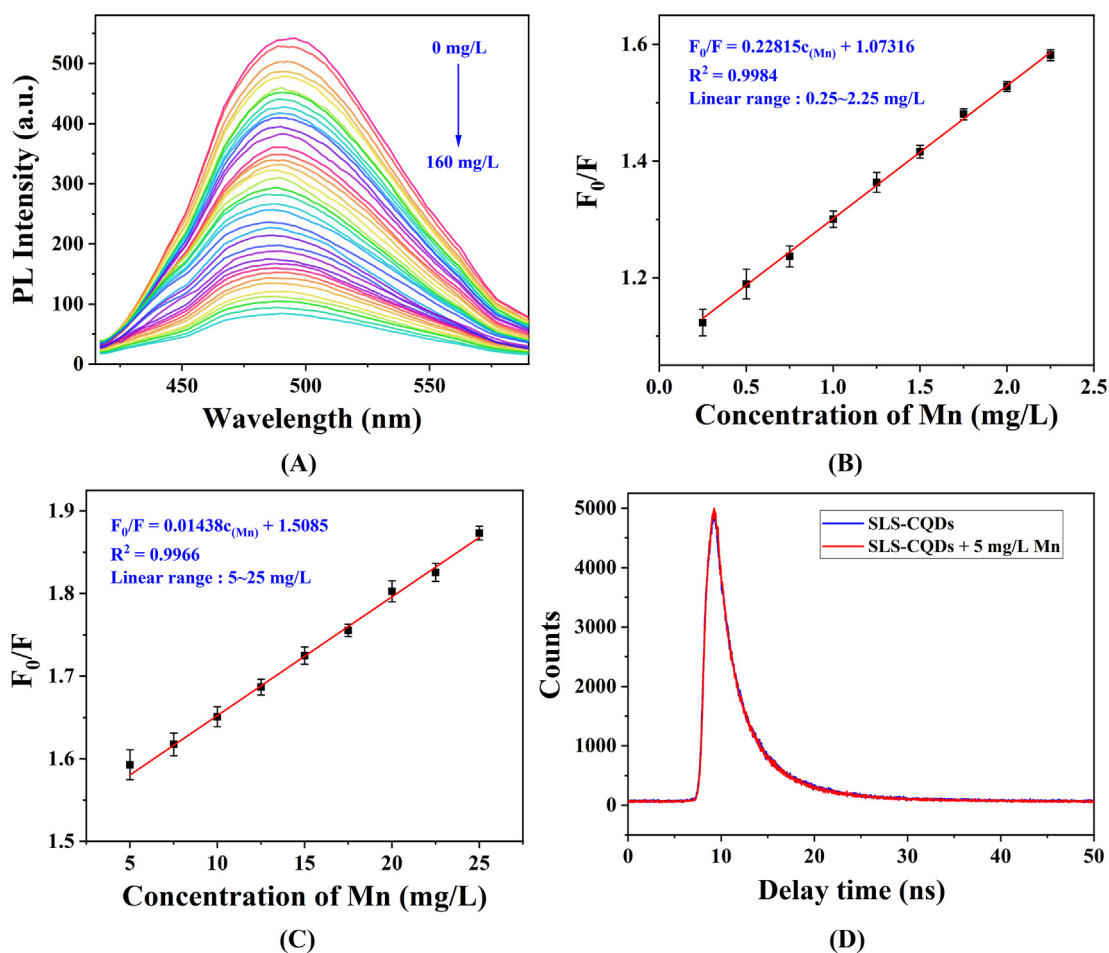


Fig. 4 (A) Fluorescence quenching of SLS-CQDs in the presence of Mn (0–160 mg/L). The linear relationship between the fluorescence intensity of the SLS-CQDs (1.0 mg/L) and the concentration of Mn in the range of (B) 0.25–2.25 mg/L and (C) 5.0–25.0 mg/L. F_0/F indicates the ratio of the fluorescence intensity of the SLS-CQDs in the absence of Mn to that in the presence of Mn. (D) The fluorescence decay curve of SLS-CQDs (1.0 mg/mL) without and with Mn.

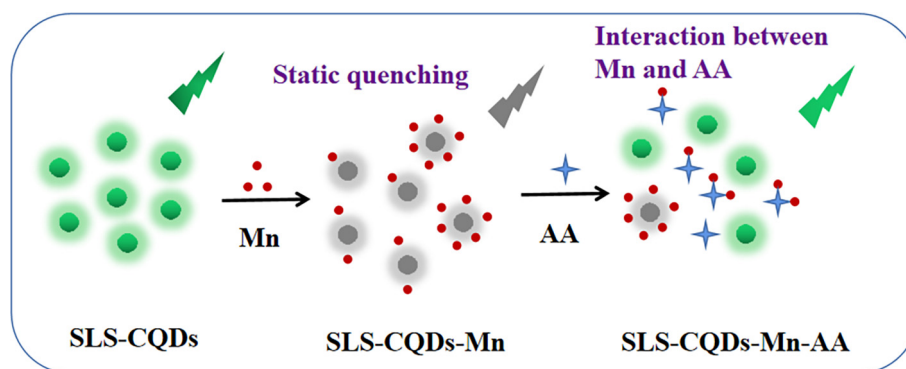
Table 1 Comparison of the proposed SLS-CQD nanoprobe with previously reported methods for detecting Mn.

Methods	Object	Linear range (mg/L)	LOD ($\mu\text{g/L}$)	Ref.
Flame AAS	Mn	0.0024–0.1	0.7	(Lemos et al., 2009)
Graphite furnace AAS	Mn	–	4.1	(Tokman et al., 2004)
ICP-AES	Mn	0.0075–10	2.2	(Manousi et al., 2022)
ICP-MS	Mn	0.02–2	0.62	(Wu et al., 2021)
Electrochemiluminescence	Mn(VII)	0.0055–16.5	4.4	(Qiu et al., 2011)
Colorimetric determination	Mn(II)	0.0055–0.275	2.86	(Najeeb et al., 2018)
Phosphorescence detection	Mn(VII)	0.0275–5.5	13.2	(Deng et al., 2017)
Fluorescent oligomer detection	Mn(VII)	0–6.6	21.6	(Ding et al., 2017a)
Fluorescent CQDs detection	Mn(VII)	0.55–11	2.66	(Du et al., 2018a)
	Mn(VII)	0.00275–5.5	0.7	(Hu et al., 2020)
	Mn	0.25–2.5, 5–25	6.9	This work

and further liberating surface-attached functionalities from Mn complexation. The recovered fluorescence of SLS-CQDs-Mn was directly related to the content of AA, which contributed to the application of SLS-CQDs-Mn in the detection of AA. The chelation effect between Mn and AA was previously reported (Gong et al., 2017b). However, when SLS-CQDs were paired with a large amount of Mn, it was more dif-

ficult for AA to capture; thus, showing no recovery at high concentrations (Scheme 2).

Based on this perspective, a nanoprobe for detecting AA was established. In the SLS-CQDs-Mn system, the suitable concentration of Mn was 30 mg/L (Fig. S10A) with an incubation time of 2 min (Fig. S10B). With the addition of AA, the fluorescence intensity of SLS-CQDs increased partially



Scheme 2 The potential mechanism of “on–off–on” for determining Mn and AA by SLS-CQDs.

(Fig. 5A). Finally, the recovery rate was almost 70 % when 150 μM AA was added to the sensing system, indicating that the testing system could not be cycled in this study. From the titration trend diagram of AA (Fig. 5B), an excellent linear relationship in the range of 5–110 μM was observed (Fig. 5C).

The limit of detection (LOD) of AA was calculated to be 0.65 μM . Compared to other fluorescence methods for the detection of AA (Table 2), the constructed sensor had a low LOD, which was comparable to the LOD of the previous methods or better than most fluorescence sensors reported.

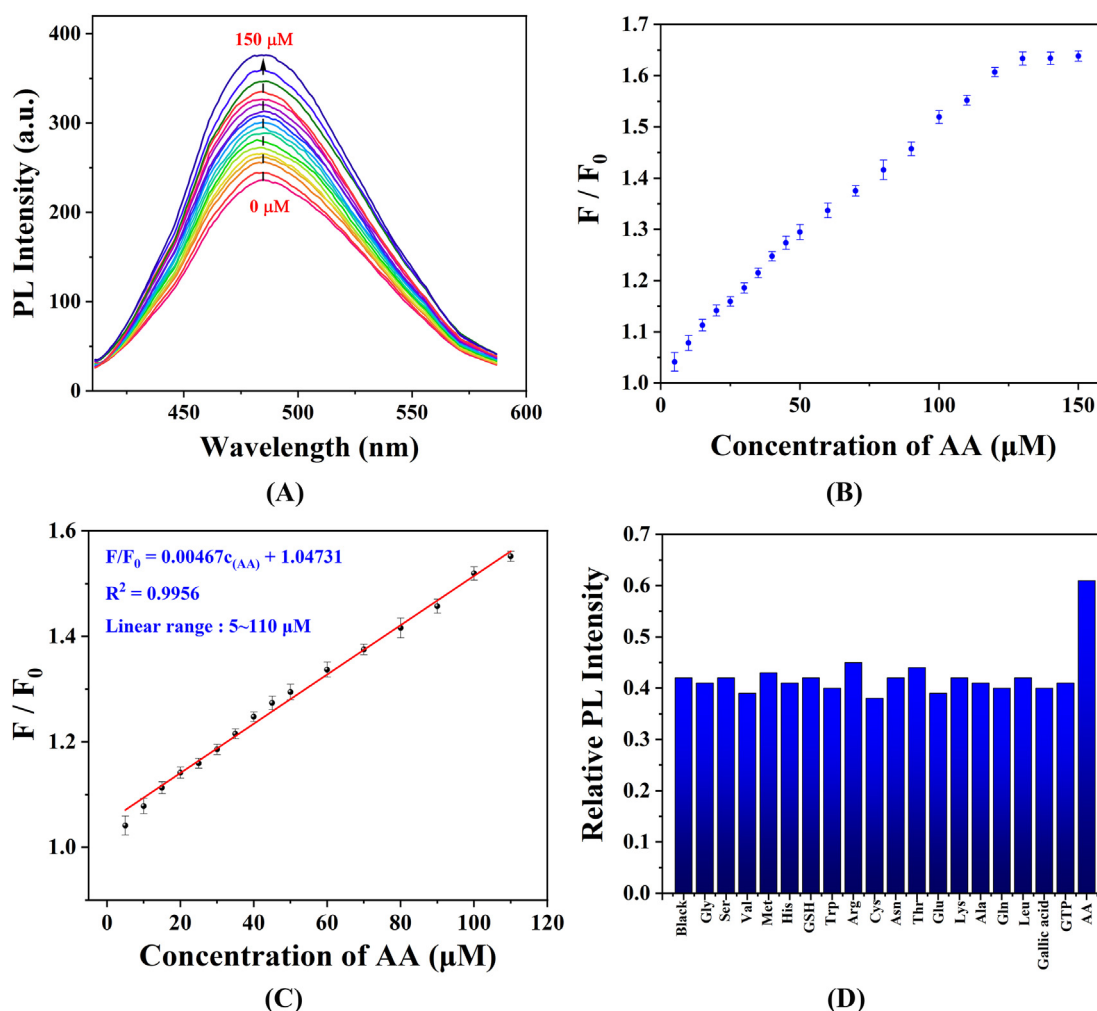


Fig. 5 (A) The fluorescence responses of the SLS-CQDs-Mn system to different concentrations of AA. (B) The titration trend diagram of SLS-CQDs-Mn at various concentrations of AA (0–150 μM). F/F_0 is the ratio of the fluorescence intensity of the SLS-CQDs-Mn in the presence of AA to that in the absence of AA. (C) The linear relationship between F/F_0 and AA concentration in the range of 5–110 μM . (D) Selectivity of the SLS-CQDs-Mn system for detecting AA.

Table 2 Comparison of previously reported fluorescence methods for AA detection with the method in this study.

Nanomaterial	Linear range (μM)	LOD (μM)	Ref.
N,S,P-CND _{Sac}	0.5–120	1.2	(Gong et al., 2017b)
Water-soluble CDs	5–350	3.11	(Wang et al., 2021)
CDs-SiO ₂	0–70	3.17	(Zhao et al., 2021)
Mn-CDs	3–140	0.9	(Chu et al., 2020)
N-doped CDs	0–150	0.02	(Lv et al., 2020)
SLS-CQDs	5–100	0.65	This work

Table 3 The analytical results for the detection of Mn in water samples.

Water Samples	Initial amount (mg/L)	Added (mg/L)	Detected (mg/L)	RSD (% , n = 6)	Recovery (%)
1	0.11	2	2.08	3.85	98.50
2	0.18	2	2.11	2.78	96.33
3	0.21	2	2.25	4.03	102.17
4	0.17	2	2.13	3.12	98.17
5	0.24	2	2.19	2.94	97.33

Table 4 The analytical results for the detection of AA in VC effervescent tablets.

VC Samples	Initial amount (mg/g)	Found in solution (μM)	Added (μM)	Detected (μM)	RSD (% , n = 6)	Recovery (%)
1	108.82	26.09	20	45.82	4.25	98.65
2	107.41	25.74	20	45.82	3.64	100.40
3	109.27	26.25	20	45.94	4.35	98.45
4	109.91	26.37	20	45.82	5.02	97.25
5	108.52	26.05	20	45.36	5.31	96.55

The detection response time of SLS-CQDs to Mn and AA, as shown in Table S3, was 5 min and 2 min, respectively. These values were considerably different from those of other research systems (Ding et al., 2017b; Dong et al., 2021b; Du et al., 2018b; Gong et al., 2017a). Gly, Ser, Val, Met, His, GSH, Trp, Arg, Cys, Asn, Thr, Glu, Lys, Ala, Gln, Leu, Gallic acid, and GTP were selected to measure the selectivity for determining AA. No noticeable enhancement effects were observed (Fig. 5D), showing good selectivity and anti-interference of the AA sensor. Our results implied that the SLS-CQDs-Mn “turn-on” fluorescence nanoprobe is an ideal sensing platform for the detection of AA.

3.6. Detection of Mn and AA in actual samples

To evaluate the feasibility of the proposed fluorescence sensing method, the analysis of Mn and AA in the actual samples was conducted according to the proposed method.

As depicted in Table 3, the sample recoveries were 96.33 %–102.17 % with the relative standard deviation (RSDs) between 2.78 % and 4.03 % (n = 6) in water samples. This demonstrated the reliability of the sensing platform detecting Mn. The SLS-CQDs-Mn fluorescent sensing platform was applied to detect AA in the VC effervescent tablets, and the results are shown in Table 4. The specification of the VC effervescent tablets showed that each VC tablet weighed about 4.2 g and contained 460 mg of AA. As shown in Table 4, the initial amount of AA in the VC effervescent tablets were 108.82,

107.41, 109.27, 109.91, and 108.52 mg/g, respectively, which fit the instruction. The quantitative spike recoveries ranged from 96.55 % to 100.40 %, with an RSD of less than 5.31 % (n = 6). These results showed that the sensing platform could provide reliable data for the detection of AA in actual samples.

4. Conclusion

To summarize, sodium lignosulfonate-derived carbon quantum dots (SLS-CQDs) were fabricated by a facile and sustainable one-step hydrothermal method. The as-prepared SLS-CQDs had excellent chemical and optical stabilities. An “on-off-on” nanoprobe for selective and sensitive detection of total Mn and AA was established. The determination of Mn was based on the static quenching process, and the detection of AA was according to the competition between SLS-CQDs and AA. The proposed fluorescence method has many advantages for detecting Mn and AA, such as a wide linear range, low LOD, high selectivity, simplicity, and fast analysis. The availability of the nanoprobe was verified by surveying the content of total Mn and AA in samples. The as-constructed SLS-CQDs might be used in various applications, which include fluorescence nanoprobe, environmental water quality monitoring, and food sample testing.

CRedit authorship contribution statement

Tingyu Zhang: Conceptualization, Methodology, Software, Data curation, Writing – original draft. **Xiaojuan Gong:** Supervision. **Yi Zhang:** Software, Validation, Funding acquisition.

Funding

This work was supported by the Scientific and Technological Innovation Programs of Higher Education Institutions in Shanxi [grant number 2019L0946]; and the Key Research Program of Lyuliang City [grant number GXZDYF2019087].

Declaration of Competing Interest

The authors declare that they have no known competing financial interests or personal relationships that could have appeared to influence the work reported in this paper.

Appendix A. Supplementary material

Supplementary data to this article can be found online at <https://doi.org/10.1016/j.arabj.2022.104422>.

References

- Abdolmohammad-Zadeh, H., Sadeghi, G.H., 2012. A nano-structured material for reliable speciation of chromium and manganese in drinking waters, surface waters and industrial wastewater effluents. *Talanta* 94, 201–208. <https://doi.org/10.1016/j.talanta.2012.03.022>.
- Aro, T., Fatehi, P., 2017. Production and Application of Lignosulfonates and Sulfonated Lignin. *ChemSusChem* 10 (9), 1861–1877. <https://doi.org/10.1002/cssc.201700082>.
- Carrier, M., Joubert, J.E., Danje, S., Hugo, T., Gorgens, J., Knoetze, J.H., 2013. Impact of the lignocellulosic material on fast pyrolysis yields and product quality. *Bioresour Technol* 150, 129–138. <https://doi.org/10.1016/j.biortech.2013.09.134>.
- Chao, D., Chen, J., Dong, Q., Wu, W., Qi, D., Dong, S., 2020. Ultrastable and ultrasensitive pH-switchable carbon dots with high quantum yield for water quality identification, glucose detection, and two starch-based solid-state fluorescence materials. *Nano Res.* 13 (11), 3012–3018. <https://doi.org/10.1007/s12274-020-2965-8>.
- Chen, W., Hu, C., Yang, Y., Cui, J., Liu, Y., 2016. Rapid synthesis of carbon dots by hydrothermal treatment of lignin. *Materials (Basel)* 9 (3). <https://doi.org/10.3390/ma9030184>.
- Chen, F., Zhou, W., Yao, H., et al, 2013. Self-assembly of NiO nanoparticles in lignin-derived mesoporous carbons for supercapacitor applications. *Green Chemistry* 15 (11). <https://doi.org/10.1039/c3gc41080c>.
- Chu, X., Ning, G., Zhou, Z., Liu, Y., Xiao, Q., Huang, S., 2020. Bright Mn-doped carbon dots for the determination of permanganate and L-ascorbic acid by a fluorescence on-off-on strategy. *Microchim. Acta* 187 (12), 1–11. <https://doi.org/10.1007/s00604-020-04604-0>.
- Deng, P., Lu, L.Q., Cao, W.C., Tian, X.K., 2017. Phosphorescence detection of manganese(VII) based on Mn-doped ZnS quantum dots. *Spectrochim. Acta A Mol. Biomol. Spectrosc.* 173, 578–583. <https://doi.org/10.1016/j.saa.2016.10.032>.
- Ding, H., Cheng, L.W., Ma, Y.Y., Kong, J.L., Xiong, H.M., 2013. Luminescent carbon quantum dots and their application in cell imaging. *New J. Chem.* 37 (8), 2515–2520. <https://doi.org/10.1039/C3NJ00366C>.
- Ding, P., Xin, X., Zhao, L., et al, 2017a. On-off-on fluorescent oligomer as a chemosensor for the detection of manganese (VII), sulfur (II) and aldehydes based on the inner filter effect. *RSC Adv.* 7 (6), 3051–3058. <https://doi.org/10.1039/C6RA25583C>.
- Ding, P., Xin, X., Zhao, L., et al, 2017b. On-off-on fluorescent oligomer as a chemosensor for the detection of manganese(vii), sulfur(ii) and aldehydes based on the inner filter effect. *RSC Adv.* 7 (6), 3051–3058. <https://doi.org/10.1039/c6ra25583c>.
- Dong, Y., Pang, H., Yang, H.B., et al, 2013. Carbon-based dots co-doped with nitrogen and sulfur for high quantum yield and excitation-independent emission. *Angew. Chem. Int. Ed. Engl.* 52 (30), 7800–7804. <https://doi.org/10.1002/anie.201301114>.
- Dong, W., Yu, J., Gong, X., Liang, W., Fan, L., Dong, C., 2021. A turn-off-on near-infrared photoluminescence sensor for sequential detection of Fe(3+) and ascorbic acid based on glutathione-capped gold nanoclusters. *Spectrochim. Acta A Mol. Biomol. Spectrosc.* 247,. <https://doi.org/10.1016/j.saa.2020.119085> 119085.
- Du, F., Li, G., Gong, X., et al, 2018a. Facile, rapid synthesis of N, P-dual-doped carbon dots as a label-free multifunctional nanosensor for Mn (VII) detection, temperature sensing and cellular imaging. *Sens. Actuata. B Chem.* 277, 492–501. <https://doi.org/10.1016/j.snb.2018.09.027>.
- Du, F., Li, G., Gong, X., et al, 2018b. Facile, rapid synthesis of N, P-dual-doped carbon dots as a label-free multifunctional nanosensor for Mn(VII) detection, temperature sensing and cellular imaging. *Sensors and Actuators B: Chemical* 277, 492–501. <https://doi.org/10.1016/j.snb.2018.09.027>.
- Gao, D., Liu, A., Zhang, Y., et al, 2021. Temperature triggered high-performance carbon dots with robust solvatochromic effect and self-quenching-resistant deep red solid state fluorescence for specific lipid droplet imaging. *Chem. Eng. J.* 415,. <https://doi.org/10.1016/j.cej.2021.128984> 128984.
- Georgakilas, V., Perman, J.A., Tucek, J., Zboril, R., 2015. Broad family of carbon nanoallotropes: classification, chemistry, and applications of fullerenes, carbon dots, nanotubes, graphene, nanodiamonds, and combined superstructures. *Chem. Rev.* 115 (11), 4744–4822. <https://doi.org/10.1021/cr500304f>.
- Goldhaber, S.B., 2003. Trace element risk assessment: essentiality vs. toxicity. *Regul. Toxicol. Pharmacol.* 38 (2), 232–242. [https://doi.org/10.1016/s0273-2300\(02\)00020-x](https://doi.org/10.1016/s0273-2300(02)00020-x).
- Gong, X., Lu, W., Liu, Y., et al, 2015a. Low temperature synthesis of phosphorous and nitrogen co-doped yellow fluorescent carbon dots for sensing and bioimaging. *J. Mater. Chem. B* 3 (33), 6813–6819. <https://doi.org/10.1039/c5tb00575b>.
- Gong, X., Lu, W., Paa, M.C., et al, 2015b. Facile synthesis of nitrogen-doped carbon dots for Fe(3+) sensing and cellular imaging. *Anal. Chim. Acta* 861, 74–84. <https://doi.org/10.1016/j.aca.2014.12.045>.
- Gong, X., Zhang, Q., Gao, Y., Shuang, S., Choi, M.M., Dong, C., 2016. Phosphorus and Nitrogen Dual-Doped Hollow Carbon Dot as a Nanocarrier for Doxorubicin Delivery and Biological Imaging. *ACS Appl. Mater. Interfaces* 8 (18), 11288–11297. <https://doi.org/10.1021/acsami.6b01577>.
- Gong, X., Li, Z., Hu, Q., Zhou, R., Shuang, S., Dong, C., 2017. N, S, P Co-Doped carbon nanodot fabricated from waste microorganism and its application for label-free recognition of Manganese(VII) and l-Ascorbic Acid and AND logic gate operation. *ACS Appl. Mater. Interfaces* 9 (44), 38761–38772. <https://doi.org/10.1021/acsami.7b11170>.
- Gong, X., Wang, H., Liu, Y., et al, 2019. A di-functional and label-free carbon-based chem-nanosensor for real-time monitoring of pH fluctuation and quantitative determining of Curcumin. *Anal. Chim. Acta* 1057, 132–144. <https://doi.org/10.1016/j.aca.2019.01.012>.
- Hu, Q., Meng, X., Chan, W., 2016. An investigation on the chemical structure of nitrogen and sulfur codoped carbon nanoparticles by ultra-performance liquid chromatography-tandem mass spectrometry. *Anal. Bioanal. Chem.* 408 (19), 5347–5357. <https://doi.org/10.1007/s00216-016-9631-8>.
- Hu, Q., Liu, L., Sun, H., et al, 2020. An ultra-selective fluorescence method with enhanced sensitivity for the determination of manganese (VII) in food stuffs using carbon quantum dots as nanoprobe. *J. Food Compos. Anal.* 88,. <https://doi.org/10.1016/j.jfca.2020.103447> 103447.
- Jiang, K., Sun, S., Zhang, L., et al, 2015. Red, green, and blue luminescence by carbon dots: full-color emission tuning and multicolor cellular imaging. *Angew. Chem. Int. Ed. Engl.* 54 (18), 5360–5363. <https://doi.org/10.1002/anie.201501193>.

- Joshi, P., Nair, M., Kumar, D., 2016. pH-controlled sensitive and selective detection of Cr(III) and Mn(II) by using clove (*S. aromaticum*) reduced and stabilized silver nanospheres. *Analytical Methods* 8 (6), 1359–1366. <https://doi.org/10.1039/c5ay03217b>.
- Kai, D., Tan, M.J., Chee, P.L., Chua, Y.K., Yap, Y.L., Loh, X.J., 2016. Towards lignin-based functional materials in a sustainable world. *Green Chem.* 18 (5), 1175–1200. <https://doi.org/10.1039/C5GC02616D>.
- Kibet, J., Khachatryan, L., Dellinger, B., 2012. Molecular products and radicals from pyrolysis of lignin. *Environ. Sci. Technol.* 46 (23), 12994–13001. <https://doi.org/10.1021/es302942c>.
- Kong, W., Liu, J., Liu, R., et al., 2014. Quantitative and real-time effects of carbon quantum dots on single living HeLa cell membrane permeability. *Nanoscale* 6 (10), 5116–5120. <https://doi.org/10.1039/c3nr06590a>.
- Kumar, D., Nair, M., Painuli, R., 2019. Highly responsive bioinspired AgNPs probe for the precise colorimetric detection of the Mn (II) in aqueous systems. *Plasmonics* 14 (2), 303–311. <https://doi.org/10.1007/s11468-018-0805-4>.
- Lemos, V.A., Novaes, C.G., Bezerra, M.A., 2009. An automated preconcentration system for the determination of manganese in food samples. *J. Food Compos. Anal.* 22 (4), 337–342. <https://doi.org/10.1016/j.jfca.2008.11.019>.
- Li, N., Li, Y., Han, Y., Pan, W., Zhang, T., Tang, B., 2014. A highly selective and instantaneous nanoprobe for detection and imaging of ascorbic acid in living cells and in vivo. *Anal. Chem.* 86 (8), 3924–3930. <https://doi.org/10.1021/ac5000587>.
- Li, Y., Ren, J., Sun, R., Wang, X., 2018. Fluorescent Lignin Carbon Dots for Reversible Responses to High-Valence Metal Ions and Its Bioapplications. *J. Biomed. Nanotechnol.* 14 (9), 1543–1555. <https://doi.org/10.1166/jbn.2018.2610>.
- Liao, X., Chen, C., Zhou, R., et al., 2020. Comparison of N-doped carbon dots synthesized from the main components of plants including cellulose, lignin, and xylose: characterized, fluorescence mechanism, and potential applications. *Dyes Pigm.* 183, <https://doi.org/10.1016/j.dyepig.2020.108725> 108725.
- Liu, J., Li, J., Xu, L., Qiao, Y., Chen, J., 2017b. Facile synthesis of N, B-doped carbon dots and their application for multisensor and cellular imaging. *Ind. Eng. Chem. Res.* 56 (14), 3905–3912. <https://doi.org/10.1021/acs.iecr.6b04752>.
- Liu, F., Li, H., Liao, D., et al., 2020a. Carbon quantum dots derived from the extracellular polymeric substance of anaerobic ammonium oxidation granular sludge for detection of trace Mn(VII) and Cr(VI). *RSC Adv.* 10 (53), 32249–32258. <https://doi.org/10.1039/d0ra06133f>.
- Liu, Y., Liu, Y., Park, S.J., et al., 2015. One-step synthesis of robust nitrogen-doped carbon dots: acid-evoked fluorescence enhancement and their application in Fe³⁺ detection. *J. Mater. Chem. A* 3 (34), 17747–17754. <https://doi.org/10.1039/C5TA05189D>.
- Liu, B., Peng, T., Sun, H., 2017a. Leaching behavior of U, Mn, Sr, and Pb from different particle-size fractions of uranium mill tailings. *Environ. Sci. Pollut. Res. Int.* 24 (18), 15804–15815. <https://doi.org/10.1007/s11356-017-8921-9>.
- Liu, S., Tian, J., Wang, L., et al., 2012. Hydrothermal treatment of grass: a low-cost, green route to nitrogen-doped, carbon-rich, photoluminescent polymer nanodots as an effective fluorescent sensing platform for label-free detection of Cu(II) ions. *Adv. Mater.* 24 (15), 2037–2041. <https://doi.org/10.1002/adma.201200164>.
- Liu, Y., Yang, H., Ma, C., et al., 2020b. Luminescent Transparent Wood Based on Lignin-Derived Carbon Dots as a Building Material for Dual-Channel, Real-Time, and Visual Detection of Formaldehyde Gas. *ACS Appl. Mater. Interfaces* 12 (32), 36628–36638. <https://doi.org/10.1021/acsami.0c10240>.
- Lv, X., Man, H., Dong, L., Huang, J., Wang, X., 2020. Preparation of highly crystalline nitrogen-doped carbon dots and their application in sequential fluorescent detection of Fe³⁺ and ascorbic acid. *Food Chem.* 326, <https://doi.org/10.1016/j.foodchem.2020.126935> 126935.
- Manousi, N., Kalogiouri, N.P., Kokokiris, L., Anthemidis, A., Zachariadis, G.A., 2022. Rapid Multielemental Inductively Coupled Plasma-Atomic Emission Spectrometric (ICP-AES) Method for the Assessment of the Quality of Flower Waters. *Analyt. Lett.* 55 (1), 123–131. <https://doi.org/10.1080/00032719.2021.1919135>.
- Mohagheghpour, E., Farzin, L., Ghoorchian, A., Sadjadi, S., Abdouss, M., 2022. Selective detection of manganese(II) ions based on the fluorescence turn-on response via histidine functionalized carbon quantum dots. *Spectrochim. Acta A Mol. Biomol. Spectrosc.* 279, <https://doi.org/10.1016/j.saa.2022.121409> 121409.
- Myint, A.A., Rhim, W.K., Nam, J.M., Kim, J., Lee, Y.W., 2018. Water-soluble, lignin-derived carbon dots with high fluorescent emissions and their applications in bioimaging. *J. Ind. Eng. Chem.* 66, 387–395. <https://doi.org/10.1016/j.jiec.2018.06.005>.
- Myrvold, B.O., 2008. A new model for the structure of lignosulphonates: Part 1. Behaviour in dilute solutions. *Ind. Crops Prod.* 27 (2), 214–219. <https://doi.org/10.1016/j.indcrop.2007.07.010>.
- Najeeb, M., Zaman, M.I., Niaz, A., Nawaz, M., Bilal, M., Shah, K.H., 2018. A simple colorimetric method for the detection of Mn²⁺ based on the catalytic oxidation ability of silver nanoparticles. *Mater. Res. Express* 5, (12), <https://doi.org/10.1088/2053-1591/aae178> 125012.
- Narayanan, K.B., Han, S.S., 2017. Colorimetric detection of manganese (II) ions using alginate-stabilized silver nanoparticles. *Res. Chem. Intermed.* 43 (10), 5665–5674. <https://doi.org/10.1007/s11164-017-2954-z>.
- Nie, Q., Wang, Y., Jia, L., et al., 2017. Luminescence resonance energy transfer probes based on NaYF₄: Yb, Er-Ag nanocompounds for sensitive detection of Mn²⁺ ions. *J. Alloys Compounds* 722, 896–902. <https://doi.org/10.1016/j.jallcom.2017.06.112>.
- Niu, N., Ma, Z., He, F., et al., 2017. Preparation of Carbon Dots for Cellular Imaging by the Molecular Aggregation of Cellulolytic Enzyme Lignin. *Langmuir* 33 (23), 5786–5795. <https://doi.org/10.1021/acs.langmuir.7b00617>.
- Pan, Y.Y., Yin, W.M., Meng, R.J., Guo, Y.R., Zhang, J.G., Pan, Q.J., 2021. Productive preparation of N-doped carbon dots from sodium lignosulfonate/melamine formaldehyde foam and its fluorescence detection of trivalent iron ions. *RSC Adv.* 11 (39), 24038–24043. <https://doi.org/10.1039/d1ra03279h>.
- Pei, Y., Chang, A., Liu, X., et al., 2021. Nitrogen-doped carbon dots from Kraft lignin waste with inorganic acid catalyst and their brain cell imaging applications. *AIChE J.* 67 (5), e17132.
- Qiu, B., Xue, L., Wu, Y., Lin, Z., Guo, L., Chen, G., 2011. Mechanism study on inorganic oxidants induced inhibition of Ru(bpy)₃²⁺ electrochemiluminescence and its application for sensitive determination of some inorganic oxidants. *Talanta* 85 (1), 339–344. <https://doi.org/10.1016/j.talanta.2011.03.063>.
- Rai, S., Singh, B.K., Bhartiya, P., et al., 2017. Lignin derived reduced fluorescence carbon dots with theranostic approaches: nano-drug-carrier and bioimaging. *J. Luminescence* 190, 492–503. <https://doi.org/10.1016/j.jlumin.2017.06.008>.
- Ruan, Y., Wu, L., Jiang, X., 2016. Self-assembly of nitrogen-doped carbon nanoparticles: a new ratiometric UV-vis optical sensor for the highly sensitive and selective detection of Hg(2+) in aqueous solution. *Analyst* 141 (11), 3313–3318. <https://doi.org/10.1039/c6an00465b>.
- Song, S., Liang, F., Li, M., et al., 2019. A label-free nano-probe for sequential and quantitative determination of Cr(VI) and ascorbic acid in real samples based on S and N dual-doped carbon dots. *Spectrochim. Acta A Mol. Biomol. Spectrosc.* 215, 58–68. <https://doi.org/10.1016/j.saa.2019.02.065>.
- Sun, X., Niu, Y., Bi, S., Zhang, S., 2008. Determination of ascorbic acid in individual rat hepatocyte by capillary electrophoresis with electrochemical detection. *J. Chromatogr. B Analyt. Technol. Biomed. Life Sci.* 870 (1), 46–50. <https://doi.org/10.1016/j.jchromb.2008.05.035>.
- Tokman, N., Akman, S., Ozeroglu, C., 2004. Determination of lead, copper and manganese by graphite furnace atomic absorption

- spectrometry after separation/concentration using a water-soluble polymer. *Talanta* 63 (3), 699–703. <https://doi.org/10.1016/j.talanta.2003.12.018>.
- Upton, B.M., Kasko, A.M., 2016. Strategies for the Conversion of Lignin to High-Value Polymeric Materials: Review and Perspective. *Chem. Rev.* 116 (4), 2275–2306. <https://doi.org/10.1021/acs.chemrev.5b00345>.
- Vieira, D.R., Castro, J.T., Lemos, V.A., 2011. Determination of lead and manganese in biological samples and sediment using slurry sampling and flame atomic absorption spectrometry. *J. AOAC Int.* 94 (2), 645–649.
- Wang, T., Luo, H., Jing, X., Yang, J., Huo, M., Wang, Y., 2021. Synthesis of Fluorescent Carbon Dots and Their Application in Ascorbic Acid Detection. *Molecules* 26 (5). <https://doi.org/10.3390/molecules26051246>.
- Wang, W., Peng, J., Li, F., Su, B., Chen, X., Chen, X., 2018. Phosphorus and chlorine co-doped carbon dots with strong photoluminescence as a fluorescent probe for ferric ions. *Mikrochim. Acta* 186 (1), 32. <https://doi.org/10.1007/s00604-018-3140-8>.
- Wang, J., Wang, J., Xiao, W., et al, 2020. Lignin-derived red-emitting carbon dots for colorimetric and sensitive fluorometric detection of water in organic solvents. *Anal. Methods* 12 (25), 3218–3224. <https://doi.org/10.1039/d0ay00485e>.
- Wu, X., Keegan, J., Behan, P., 2021. Migration analysis of Cr, Ni, Al, Fe, Mn, Cu, Zn, and Mo in internet-bought food serving stainless-steel utensils by ICP-MS and XRF. *Food Addit. Contam. Part B Surveill.* 14 (4), 256–263. <https://doi.org/10.1080/19393210.2021.1946168>.
- Xu, L., Fan, H., Huang, L., et al, 2017. Eosinophilic nitrogen-doped carbon dots derived from tribute chrysanthemum for label-free detection of Fe^{3+} ions and hydrazine. *J. Taiwan Institute Chem. Engineers* 78, 247–253. <https://doi.org/10.1016/j.jtice.2017.06.011>.
- Xu, Q., Liu, X., Jiang, Y., Wang, P., 2021a. A highly sensitive and selective probe for the colorimetric detection of Mn(II) based on the antioxidative selenium and nitrogen co-doped carbon quantum dots and ABTS(*). *Front. Chem.* 9. <https://doi.org/10.3389/fchem.2021.658105> 658105.
- Xu, Q., Liu, X., Jiang, Y., Wang, P., 2021b. A highly sensitive and selective probe for the colorimetric detection of Mn(II) based on the antioxidative selenium and nitrogen Co-Doped carbon quantum dots and ABTS(●). *Front. Chem.* 9. <https://doi.org/10.3389/fchem.2021.658105> 658105.
- Xu, X., Mo, L., Li, Y., et al, 2021c. Construction of carbon dots with color-tunable aggregation-induced emission by nitrogen-induced intramolecular charge transfer. *Adv. Mater.* 33 (49), e2104872.
- Yang, X., Guo, Y., Liang, S., et al, 2020. Preparation of sulfur-doped carbon quantum dots from lignin as a sensor to detect Sudan I in an acidic environment. *J. Mater. Chem. B* 8 (47), 10788–10796. <https://doi.org/10.1039/d0tb00125b>.
- Yang, M., Liu, M., Wu, Z., et al, 2019. Carbon dots co-doped with nitrogen and chlorine for “off-on” fluorometric determination of the activity of acetylcholinesterase and for quantification of organophosphate pesticides. *Mikrochim. Acta* 186 (8), 585. <https://doi.org/10.1007/s00604-019-3715-z>.
- Zhang, H., Kang, S., Wang, G., Zhang, Y., Zhao, H., 2016. Fluorescence determination of nitrite in water using prawn-shell derived nitrogen-doped carbon nanodots as fluorophores. *ACS Sensors* 1 (7), 875–881. <https://doi.org/10.1021/acssensors.6b00269>.
- Zhang, K., Sun, P., Faye, M.C.A.S., Zhang, Y., 2018. Characterization of biochar derived from rice husks and its potential in chlorobenzene degradation. *Carbon* 130, 730–740. <https://doi.org/10.1016/j.carbon.2018.01.036>.
- Zhang, K., Sun, P., Zhang, Y., Muruganathan, M., Ammasai, K., Zhang, Y., 2020. Enhancement of S(IV)-Cr(VI) reaction in p-nitrophenol degradation using rice husk biochar at neutral conditions. *Sci Total Environ* 749. <https://doi.org/10.1016/j.scitotenv.2020.142086> 142086.
- Zhao, T., Zhu, C., Xu, S., et al, 2021. Fluorescent color analysis of ascorbic acid by ratiometric fluorescent paper utilizing hybrid carbon dots-silica coated quantum dots. *Dyes Pigm.* 186. <https://doi.org/10.1016/j.dyepig.2020.108995> 108995.
- Zhu, S., Khan, M.A., Kameda, T., et al, 2022. New insights into the capture performance and mechanism of hazardous metals Cr^{3+} and Cd^{2+} onto an effective layered double hydroxide based material. *J Hazard Mater* 426. <https://doi.org/10.1016/j.jhazmat.2021.128062> 128062.
- Zhu, H., Luo, W., Ciesielski, P.N., et al, 2016. Wood-derived materials for green electronics, biological devices, and energy applications. *Chem. Rev.* 116 (16), 9305–9374. <https://doi.org/10.1021/acs.chemrev.6b00225>.
- Zhu, L., Shen, D., Wang, Q., Luo, K.H., 2021. Green synthesis of tunable fluorescent carbon quantum dots from lignin and their application in anti-counterfeit printing. *ACS Appl. Mater. Interfaces* 13 (47), 56465–56475. <https://doi.org/10.1021/acsaami.1c16679>.
- Zhu, S., Xia, M., Chu, Y., et al, 2019. Adsorption and Desorption of Pb(II) on l-Lysine Modified Montmorillonite and the simulation of Interlayer Structure. *Appl. Clay Sci.* 169, 40–47. <https://doi.org/10.1016/j.clay.2018.12.017>.
- Zu, F., Yan, F., Bai, Z., et al, 2017. The quenching of the fluorescence of carbon dots: a review on mechanisms and applications. *Mikrochim. Acta* 184 (7), 1899–1914. <https://doi.org/10.1007/s00604-017-2318-9>.